Solid Freeform Fabrication 2022: Proceedings of the 33rd Annual International Solid Freeform Fabrication Symposium – An Additive Manufacturing Conference
Reviewed Paper

A Model for the Effects of Driving Signal on Piezoelectric Inkjet Printing Speed

Chao Sui, Wenchao Zhou

The AM^3 Lab, Department of Mechanical Engineering, University of Arkansas
Fayetteville, AR, USA; Corresponding email: zhouw@uark.edu

Piezo drop-on-demand (DOD) inkjet is a non-contact and direct forming technique for pattern fabrication, which has been widely used in additive manufacturing and other industrial applications. It is known that the ink properties and the waveform of the driving signal play a significant role in droplet ejection behavior. In this paper, we present a model for the droplet formation dynamics from a single nozzle with a bipolar driving signal, which provides a quantitative relationship between the waveform of the driving signal and the average jetting velocity at the nozzle exit, droplet ejection frequency, droplet volume, and printing speed. An experimental setup is developed for calibration and validation of the model. Results show the model agrees well with experiments and can be used to predict inkjet printing speed based on the parameters of the driving signal.

Keywords: piezo inkjet, printing speed, drop-on-demand (DOD), driving signal, model

I. INTRODUCTION

Additive manufacturing (AM) is a process of joining materials layer by layer to build 3D structures [1]. It has shown great promise as a digital manufacturing technique for a variety of reasons, such as more freedom to design and innovate, less time required from initial design to manufacturing, less material waste, and capability to manufacture with multiple materials. Many industries including medical, aerospace, and automotive are embracing the advantages of AM and implementing this technology successfully [2-4] . However, the printing speed of AM, when compared to traditional manufacturing, such as injection molding, is relatively slow, which impedes its adoption for mass production. Many different 3D printing technologies have been developed to improve the printing speed. A significant transition is from point-wise printing to line-wise or layer-wise printing. Inkjet 3D printing shows promise of scalability in printing speed with parallel printing using multiple nozzles. While inkjet printing speed has been improved over the past decades [6], its printing speed is still relatively slow when compared with traditional manufacturing methods. For example, existing industrial inkjet printheads (e.g., Sapphire QS-256/10 AAA from FUJIFILM) typically print at a build rate of ~500 cm^3/hour [7] while the comparable-size injection molding machine typically have a build rate over 15,000 cm^3/hour [8].

Numerous efforts have been devoted to improve the printing speed of inkjet, which has increased significantly over the past decades, dubbed as “Moore’s law for inkjet printing” [9]. There are typically three ways to improve the DOD inkjet printing speed as illustrated in Figure 1: more nozzles, larger droplet size, or higher printing frequency (defined as the number of droplets ejected per second per nozzle).

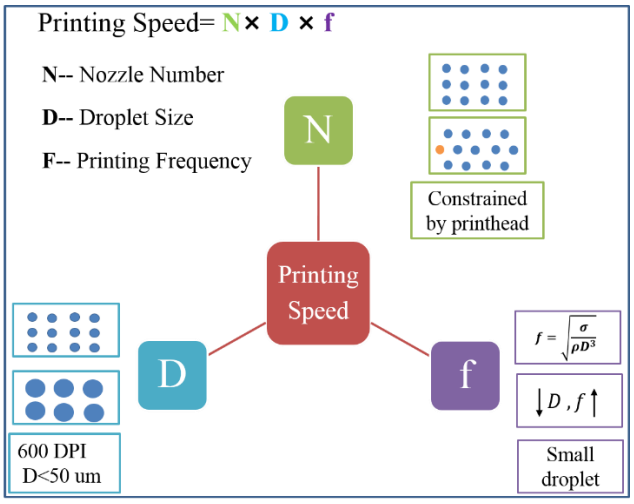

Figure 1 Explanation for the factors and their effects on the printing speed

The majority of the inkjet speed increase over the past decades comes from adding more nozzles on the printhead. For example, MEMJET has successfully developed a single pass printhead with a staggering 70,000 nozzles [10]. However, this path is coming to an end, as the number of nozzles is constrained by the size of the printhead and the maximum nozzle density. Another approach is by increasing droplet size, which is limited by two factors, printing resolution and nozzle size. For instance, to achieve a 600 DPI (dot per inch) resolution, the droplet diameter needs to be smaller than ~50μm. In addition, because the droplet size is usually commensurate with the nozzle size [11], therefore, larger nozzles are typically needed to obtain big droplet, which means fewer nozzles can be included per unit area in the printhead.

Many efforts have been made on manipulating the driving signal to generate different size droplets [12-21]. One common conclusion is that the ejected droplet volume increases with the voltage amplitude of the driving signal, which, however, often leads to satellite droplets and is not desirable for printing accuracy. Besides, it is found an optimum dwell time exists for achieving the highest drop volume for a given amplitude pulse [13, 22, 23]. This optimal dwell time varies for different experiment setups, which has been explained by the acoustic wave propagation and reflection theory. For example, the optimal value for a squeeze model piezo inkjet device is defined as L/c, where L is the cavity length, c is the sound speed in the dispensed solution. Self and Wallace [24] demonstrated the feasibility of generating droplets with radius up to two times of the radius of the nozzle by using a very long transition/dwell time waveform with higher voltage. But their method significantly increased the time used for energy input, which sacrifices the ejection frequency (from 15 kHz to 1 kHz). Therefore, the overall printing speed is decreased. It is also found that the time interval between two consecutive pulses has a significant effect on the droplet size. For instance, Shin et al. [23] found the longer separation in a double-pulse waveform produced a bigger droplet, but droplet size was still smaller than the nozzle size. Similar results were also reported by Y. Kim et al [25].

For the printing frequency, the commercial inkjet printer typically prints at the frequency of ~10s kHz. This is because the droplet generation in current inkjet printers is primarily

driven by the surface tension of the ink, which puts a limit of the droplet generation frequency to ~10s kHz for a ~50 μm sized droplet and can be estimated by [26]:

$$f = \sqrt{\frac{\sigma}{\rho D^3}} \quad (1)$$

where σ is the surface tension of the ink, ρ is the density of the ink, D is the nozzle diameter. Therefore, a smaller nozzle is needed for higher frequency, which typically leads to smaller droplet size and does not improve the overall printing speed.

While the existing research has provided insights into the important factors that can affect different aspects of printing speed (e.g., nozzle number, droplet size, jetting frequency), no systematic study has been conducted on how to increase the overall printing speed, considering of the tradeoff between different factors (e.g., jetting frequency vs. droplet size). Further, there exists no model that can provide an understanding of how the driving signal and printhead parameters affect the printing speed. This paper fills this gap by providing a systematic study for modeling the effects of the driving signal on the ejected droplet volume, jetting frequency, and printing speed. First, a low-cost piezo droplet generation system was developed to provide an experimental setup for the study. A model is developed to predict the effects of the driving signal and the printhead parameters on the printing speed. Experimental tests were then performed to calibrate the model coefficients and validate the model. Results show the model can effectively predict the effects the driving signal on printing speed.

The rest of this paper is organized as follows. In section 2, the experimental setup is presented. Section 3 presents a theoretical model for printing speed and its calibration and validation with experimental data. The effects of the signal parameters on the printing speed are studied with both the model and experiments in section 4. Conclusions are given in section 5.

II. EXPERIMENT SETUP

To perform the systematic study, we need an experimental setup that allows us to change the parameters of the waveform of the driving signal, generate droplets on demand, and observe the droplet formation process. Although many DOD systems have been reported in the literature, most of the commercially available systems are costly and do not provide the necessary freedom for us to conduct the intended study [20, 27-31]. Therefore, we designed an experimental setup with the following characteristics: (1) Low operation voltage (less than 30 V and around 1/3 of the comparable sized droplet generator voltage [20, 31]) for simpler design and safer operation; (2) A custom circuit allowing users to program arbitrary driving signal for the actuator; (3) Low cost with off-the-shelf or custom machined components.

A. Apparatus

Inspired by the design of Yang [32], we developed a simple and repeatable DOD apparatus as shown in Figure 2 (A). It consists of three subsystems: the droplet generation, observation, and control. The entire system operates as following: 1) A driving signal is programmed and generated using an Arduino board; 2) The generated signal is sent to drive a piezoelectric transducer through a custom-designed circuit (Appendix C);

3) The driving signal is observed in a oscilloscope to verify it is the desired signal; 4) The voltage of the power supply is adjusted to apply the driving signal to a piezoelectric transducer, which causes the deformation of the piezo and ejects a droplet from the nozzle; 5) A high-speed camera captures the ejection process; 6) The captured images are transported to and analyzed in a computer. The implemented setup is shown in Figure 2 (C).

The schematic of droplet generation subsystem is shown in Figure 2 (B), which mainly consists of nozzle, chamber, piezoelectric actuator, reservoir, and the elevation stage. In this paper, a 200 µm diameter, conically shaped, regular 3D printer brass nozzle is used. The piezoelectric actuator (Noliac CMBR03) has a resonant frequency of 18.4 kHz. The cylindrical chamber is custom-machined and tapers down to a tapped hole at the bottom of the chamber where the nozzle is attached. The chamber is connected to a height-adjustable reservoir through a plastic tube. Thus, the fluid pressure at the nozzle exit can be regulated to form a stable meniscus, which guarantees the repeatability of the experiments.

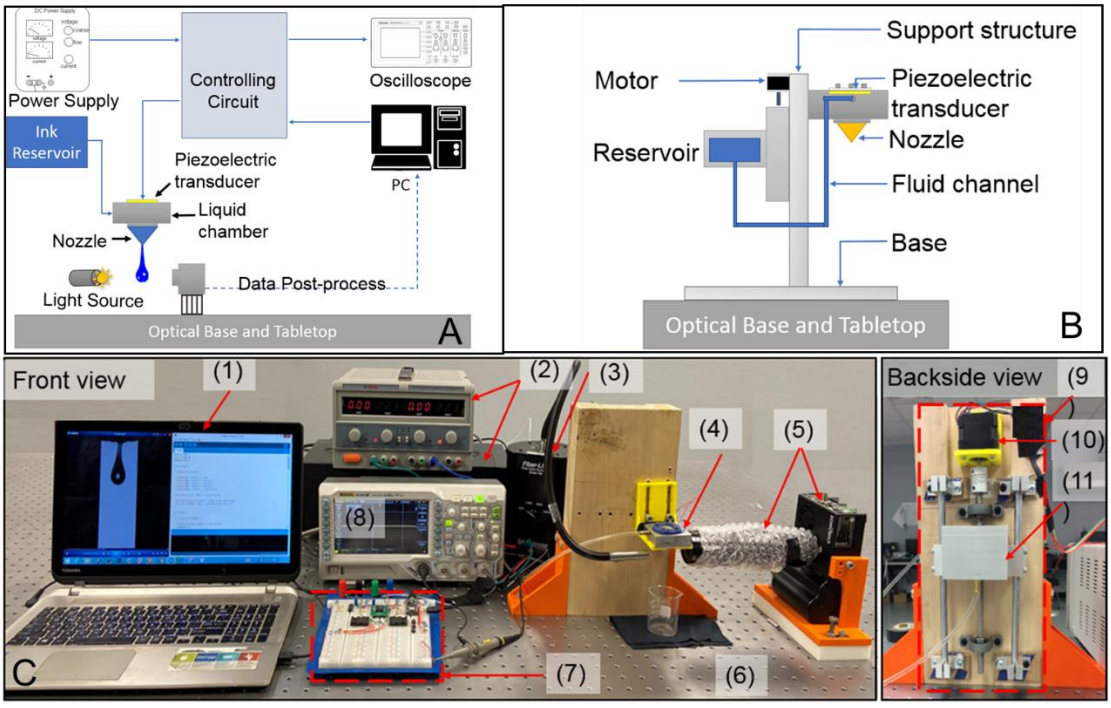

Figure 2 Experiment setup. (A) Schematic of the setup. (B) Schematic of the ink generation subsystem. (C) Setup in operation: (1) controlling computer, (2) power supply, (3) light source (Dolan-Jenner, Model 190-1), (4) generator chamber, (5) CCD high speed camera with microscope lens, (6) optical tabletop, (7) controlling circuit, (8) oscilloscope, (9) elevation stage, (10) motor, and (11) reservoir

To control the ejection process, a positive voltage is first applied, which moves the piezo down from its rest position at zero and generates a positive pressure in the chamber to force the liquid out the nozzle. When a negative voltage is applied, the piezo moves up, which generates a negative pressure in the chamber and facilitates the breakup of the droplet. This sequence of the piezo movements (down and up) expels a single droplet

from the nozzle. This sequence is programmed and controlled by the microcontroller, which can generate the designed analog signal from 0 to 5v. A custom circuit amplifies and offsets the signal to output a driving signal that varies from -45v to 45v.

To observe the ejection process, a high-speed camera with an frame rate up to 38,565 frames per second (i.e., time per frame: 26 µs) and a recording time of 4 seconds at the resolution of 640 x 96 pixels (Chronos 1.4 High Speed Camera, Kron Technologies Inc.) is used, as shown in Figure 2(C), which is sufficient to capture the droplet breakup process with the 200 µm nozzle in a single cycle. In addition, a microscope lens (-2x Barlow lens, Kron Technologies Inc.) is used to provide the necessary magnification of the droplet by adjusting the field of view, which allows achieving sufficient resolution for the droplet comparable to that being used in previous work [30, 33]. The camera records in a ring buffer in internal high-speed RAM, which stores recorded frames until full. Once full, the oldest frames are overwritten with new frames. This allows the camera to record for an unlimited period. This avoids two common issues in the often-used stroboscopic imaging of inkjet process: 1) the synchronization of the camera and the light source; 2) the variation between cycles as the jetting process is not captured in a single cycle. The camera, print head, and light source are fastened on an optical base and optical tabletop to minimize vibration.

B. Test Ink

The test ink is made of a mixture of glycerin, water and isopropanol (GWI), with a weight percentage of 34, 53, and 13 respectively. The ink is Newtonian and its properties are listed in Table 1 [34, 35] . The room temperature is maintained at 20 °C. With a nozzle diameter of 200 µm, the Ohnesorge number (Oh) is estimated to be 0.08, which is well within the printable range reported in the literature [36]. In addition, with the experimental setup, the Mach number (Ma) <0.3 and Bond number (Bo) <<1, which is within typical range of inkjet and allows the assumption of incompressible flow and negligible gravitational effect for theoretical analysis.

Table 1 Properties of test ink used in experiments

Ink	Density (g/cm^3)	Viscosity (mPa*s)	Surface tension (mN/m)
GWI	1.05	5.0	35

C. Driving Signal

With our setup, we have the freedom to program any waveform of driving signal. To facilitate the study, we chose a waveform, shown in Figure 3, as a benchmark for comparison. This bipolar driving signal resembles the driving signals typically used in the literature and can achieve a droplet size of 200 µm (equal to the nozzle size) and a jetting frequency of 2100 Hz (around the estimated theoretical limit by Equation (1))

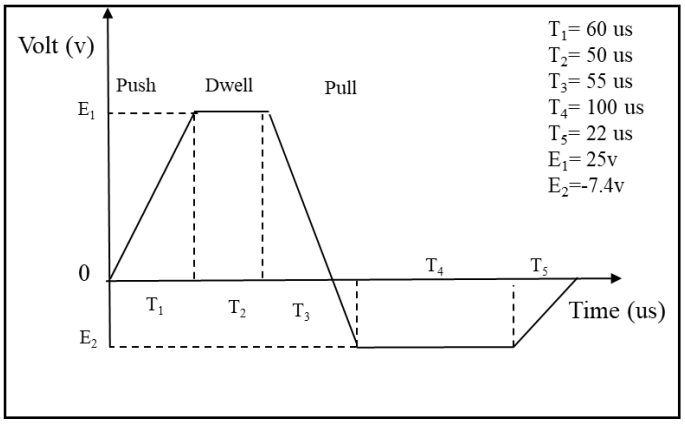

Figure 3 Benchmark signal for current setup

A jetting test is performed to validate the experimental setup with the benchmark signal and the results are shown in Figure 4: a) When the driving signal is applied, the piezo moves down and generates a positive pressure in the chamber to push the liquid out of the nozzle during T1, forming a rounded leading edge (Figure 4(1)-(2)). b) The liquid continues moving downward during T2 and starts to contract during T3 as the piezo moves up and creates a vacuum inside of chamber, slowing down the ink flow or even reversing the flow direction at the nozzle exit (Figure 4(3)). c) This leads to a velocity difference between the liquid filament head and the ink inside the nozzle, which stretches the liquid surface during T4 (Figure 4(4)). d) The piezo returns to its rest position during T5 and the ejected liquid keeps stretching until it pinches off from the nozzle (Figure 4(5)-(6)).

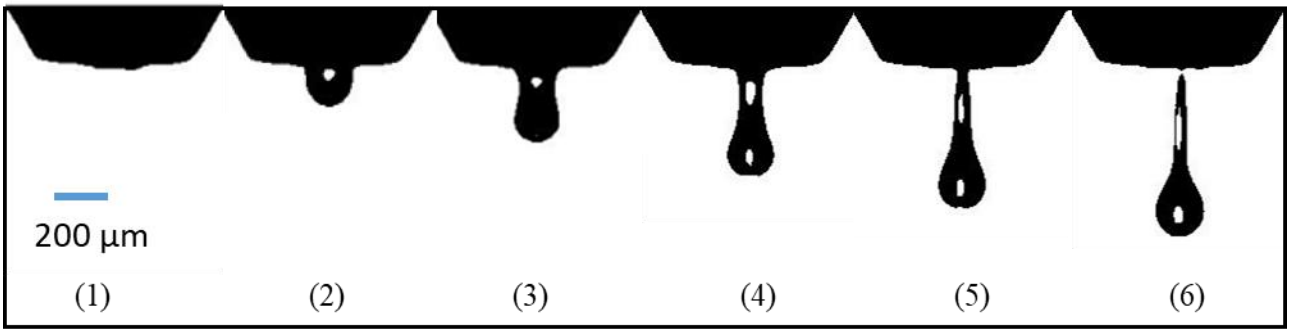

Figure 4 Experimental observation of droplet ejection using benchmark signal, the interframe time = 95us.

III. MODELING, CALIBRATION, AND VALIDATION

To understand the effects of the driving signal on the printing speed, without loss of generality, we present a model of how the parameters of a bipolar benchmark driving signal will affect printing speed. The printing speed (W), which is defined as the total volume ejected per second for one printer, can be expressed as:

$$W = N * V * f = N * \pi R^2 \int_0^{T_b} u(t)\, dt * \frac{1}{T_b} \quad (2)$$

where N is the number of nozzles, V is the volume of one droplet and can be obtained by the integration of the nozzle exit velocity u(t) over one jetting cycle, R is the filament radius at the nozzle exit during ejection, t is time, and f is the ejection frequency (defined as the number of droplets generated per second per nozzle) and equals to the reciprocal of the breakup time (Tb). Based on Equation (2), we need to know nozzle exit velocity u(t) and breakup time Tb in order to predict printing speed. In the rest of this section, we will develop a model to understand the relationship between the driving signal parameters and u(t) and Tb based on the underlying fluid mechanics.

A. Theoretical Model

1. *Nozzle Exit Velocity Estimation*

Before modeling, we need to be able to measure the nozzle exit velocity experimentally to understand its behavior, and also to validate the model later. To estimate the nozzle exit velocity u(t) experimentally, we take the average velocity in a short time period at the exit as an approximate, which can be computed in the following way (Figure 5): 1) a region of interest (ROI) is selected, where the entire ejection occurs; 2) the ejected ink volume in two instant t1 and t2 are measured and recorded as V1 and V2; 3) the average volume flow rate is calculated as: $\dot{Q} = \frac{V_2 - V_1}{t_2 - t_1}$; 4) the averaged velocity is computed through dividing the volume flow rate by the filament section area at the nozzle exit region, i.e.,

$$U(t_2) = \frac{V_2 - V_1}{\pi R_i^2 (t_2 - t_1)} \tag{3}$$

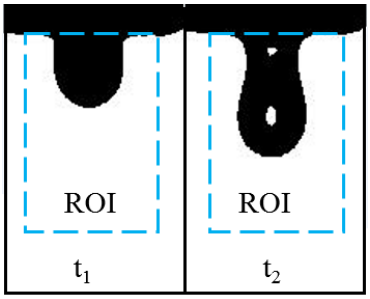

Figure 5 Ejection behavior in two instants of the region of interest (ROI): the ejection velocity is calculated by comparing the volume change at the two succeeding instants.

2. *Modeling Process*

Considering our interest is mainly in the ink flowing along the nozzle, we assume a one-dimensional model along the flow direction to simplify the analysis. First, we take one differential element at the nozzle exit as a control volume (Figure 6), where the inlet velocity is u and outlet velocity is u+Δu, the element height is Δx with the initial width of R_i. Here we define the downward direction as the positive direction (+x). Assuming gravity is negligible; the Navier-Stokes equation can be simplified as:

$$\rho\left(\frac{\partial u}{\partial t} + u\frac{\partial u}{\partial x}\right) = -\frac{\partial P}{\partial x} + f + \mu\frac{\partial^2 u}{\partial x^2} \tag{4}$$

where f is the term for external forces. After rearranging, this can be written as:

$$\rho\frac{\partial u}{\partial t} = -\frac{\partial P}{\partial x} + f + \mu\frac{\partial^2 u}{\partial x^2} - \rho u\frac{\partial u}{\partial x} \tag{5}$$

This equation indicates that the temporal acceleration (the left-hand side term) is determined by the pressure gradient, external force, viscous force, and convective inertial force. Note that all the forcing terms have dimensions of force over volume.

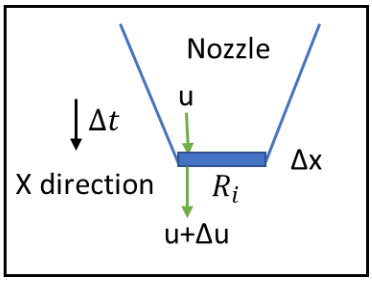

Figure 6 Sketch for the finite element analysis at the nozzle exit

The ink experiences different forces at different stages of the ejection. During T1, the piezo moves down and generates a positive pressure, which pushes the ink out of the nozzle. It is known that the magnitude of this pressure is proportional to the voltage change rate [11]. Hence, acceleration caused by the piezo can be expressed as:

$$f_{piezo} = k_1 * \frac{E_1}{T_1} \tag{6}$$

where k_1 is a constant coefficient and dependent on the piezo, E_1 is the voltage applied to piezo during T_1. The capillary pressure on the meniscus prevents ink flowing out. Based on the Young-Laplace equation, the capillary force term can be expressed as:

$$f_\sigma = \frac{k_\sigma * \sigma}{R_i} \tag{7}$$

where σ is the ink surface tension, k_σ is the coefficient measuring the acceleration caused by capillary pressure. For other terms in Eq. (5), it is convenient to express them as below [37]:

$$f_\mu = \frac{\mu\partial^2 u}{\partial x^2} = \mu\frac{\Delta(\frac{\Delta u}{\Delta x})}{\Delta x} = \frac{k_\mu \mu u}{R_i} \tag{8}$$

$$f_p = \frac{\partial P}{\partial x} + \rho u\frac{\partial u}{\partial x} = k_f \rho u^2 \tag{9}$$

where the effects of pressure gradient and inertial terms are combined and represented by the dynamic pressure because they share the same physical meaning after integration, μ is the ink viscosity, ρ is the density of ink, k_μ is the coefficient measuring the acceleration induced by viscous force, and k_f is the coefficient measuring the acceleration induced by inertial force term. Therefore, by integrating Eq. (5), the velocity estimation for T1 is:

$$u_i = u_{i-1} + \int (\frac{k_1}{\rho}\frac{E_1}{T_1} + k_f u_{i-1}^2 - \frac{k_\sigma}{\rho}\frac{\sigma}{R_i} - \frac{k_\mu u_{i-1}\mu}{\rho R_i})dt \quad (10)$$

where u_i is the velocity for current instant and u_{i-1} is the velocity in the previous time instant.

During T2, the piezo is maintained at the same position and the ink keeps flowing out. No piezo force is generated. Therefore, the velocity estimation for T2 is:

$$u_i = u_{i-1} + \int \left(k_f u_{i-1}^2 - \frac{k_\sigma}{\rho}\frac{\sigma}{R_i} - \frac{k_\mu u_{i-1}\mu}{\rho R_i}\right)dt \quad (11)$$

After T2, piezo is being moved up with the speed of voltage change rate ($\frac{E_1-E_2}{T_3}$). This gradually creates a vacuum inside the chamber, where its volume linearly increases with time. Based on Boyle's law, as volume increases, there is a proportional decrease in the pressure inside the chamber, which actually induces a stronger sucking effect for the filament. With the first order of approximation, this sucking pressure induced acceleration can be approximated as (see appendix):

$$f_n = k_n \frac{E_1 - E_2}{T_3} t \quad (12)$$

where $E_1 - E_2$ is the total voltage change during T3 for the bipolar signal, k_n is a constant coefficient measuring the acceleration caused by this sucking pressure. Therefore, the velocity estimation for T3 is:

$$u_i = u_{i-1} + \int \left(k_f u_{i-1}^2 - \frac{k_n}{\rho}\frac{E_1 - E_2}{T_3} t - \frac{k_\sigma}{\rho}\frac{\sigma}{R_i} - \frac{k_\mu u_{i-1}\mu}{\rho R_i}\right)dt \quad (13)$$

Similar to T2, the piezo is also maintained at the same position in T4 and the vacuum volume created by piezo in previous period stops increasing with time. To have a general estimation and simplify the calculation, the refill effect is neglected. Then the vacuum volume is assumed to be a constant in T4, and the pressure difference between inside the chamber and atmosphere pressure can be treated as a constant accordingly, which slows down the filament travelling and can be approximated as:

$$f_0 = k_p * P_0 \quad (14)$$

where P_0 is the atmosphere pressure, and k_p is the coefficient that measures the acceleration caused by this pressure difference. Therefore, the velocity estimation for T4 is:

$$u_i = u_{i-1} + \int \left(k_f u_{i-1}^2 - k_p * \frac{P_0}{\rho} - \frac{k_\sigma}{\rho}\frac{\sigma}{R_i} - \frac{k_\mu u_{i-1}\mu}{\rho R_i}\right)dt \quad (15)$$

In T5, piezo moves down and comes back to the original rest position, which linearly reduces the vacuum inside the chamber, which in turn decreases the pressure difference effect by introducing another force:

$$f_r = \frac{k_r}{\rho}\frac{|E_2|}{T_5}t \tag{16}$$

where E_2 is the voltage change in T5, and k_r is the coefficient that measures the acceleration caused by this piezo movement effect. Therefore, the velocity estimation for T5 is:

$$u_i = u_{i-1} + \int (k_f u_{i-1}^2 + \frac{k_r}{\rho}\frac{|E_2|}{T_5}t - k_p * \frac{P_0}{\rho} - \frac{k_\sigma}{\rho}\frac{\sigma}{R_i} - \frac{k_\mu u_{i-1}\mu}{\rho R_i})dt \tag{17}$$

After T5, signal waveform ends and no piezo force is generated. It is assumed that the vacuum is eliminated by piezo in T5. The ejection is governed by only inertial, viscous, and capillary forces:

$$u_i = u_{i-1} + \int \left(k_f u_{i-1}^2 - \frac{k_\sigma}{\rho}\frac{\sigma}{R_i} - \frac{k_\mu u_{i-1}\mu}{\rho R_i}\right)dt \tag{18}$$

Notice the filament radius in the differential element gradually decreases to zero, as the ejection approaches pinch-off. This would be used to estimate the pinch-off time. This phenomenon is modelled by applying the mass conservation to the differential element at the nozzle exit (see appendix),

$$R_i = R_{i-1} * \sqrt{1 + \frac{a_{i-1}\Delta t}{u_{i-1}}} \tag{19}$$

$$T_b = n * \Delta t \tag{20}$$

where R_{i-1} and R_i are the beginning and ending radius of Δt, a_{i-1} and u_{i-1} are the acceleration and velocity at ti-1, n is the time steps taken for radius changing from nozzle radius to zero, and T_b is the pinch-off time.

Using the known parameters (signal, ink property, nozzle size), the model for estimating the velocity at the nozzle exit, the breakup time, and the printing speed for the entire ejection cycle can be summarized as the following equations, respectively:

$u_i = u_{i-1} + \int (\frac{k_1}{\rho}\frac{E_1}{T_1} + k_f u_{i-1}^2 - \frac{k_\sigma}{\rho}\frac{\sigma}{R_i} - \frac{k_\mu u_{i-1}\mu}{\rho R_i})dt$	t in T1
$u_i = u_{i-1} + \int \left(k_f u_{i-1}^2 - \frac{k_\sigma}{\rho}\frac{\sigma}{R_i} - \frac{k_\mu u_{i-1}\mu}{\rho R_i}\right)dt$	t in T2

$u_i = u_{i-1} + \int \left(k_f u_{i-1}^2 - \frac{k_n}{\rho} \frac{E_1 - E_2}{T_3} t - \frac{k_\sigma}{\rho} \frac{\sigma}{R_i} - \frac{k_\mu u_{i-1} \mu}{\rho R_i} \right) dt$	t in T3
$u_i = u_{i-1} + \int \left(k_f u_{i-1}^2 - k_p * \frac{P_0}{\rho} - \frac{k_\sigma}{\rho} \frac{\sigma}{R_i} - \frac{k_\mu u_{i-1} \mu}{\rho R_i} \right) dt$	t in T4
$u_i = u_{i-1} + \int (k_f u_{i-1}^2 + \frac{k_r}{\rho} \frac{\lvert E_2 \rvert}{T_5} t - k_p * \frac{P_0}{\rho} - \frac{k_\sigma}{\rho} \frac{\sigma}{R_i} - \frac{k_\mu u_{i-1} \mu}{\rho R_i}) dt$	t in T5
$u_i = u_{i-1} + \int \left(k_f u_{i-1}^2 - \frac{k_\sigma}{\rho} \frac{\sigma}{R_i} - \frac{k_\mu u_{i-1} \mu}{\rho R_i} \right) dt$	After signal
$R_i = R_{i-1} * \sqrt{1 + \frac{a_i \Delta t}{u_{i-1}}} \quad T_b = n * \Delta t$	
$W = N * V * f = N * \pi R_i^2 \int_0^{T_b} u(t)\, dt * \frac{1}{T_b}$	

where T1, T2, T3, T4, T5, E1, and E2 are variables from signal, $\rho, \sigma,$ and μ are ink properties, P0 is the atmosphere pressure, k1, k_f, k_σ, k_n, k_μ, k_p, k_r are constant coefficients dependent on the experimental setup, which will be calibrated in the following section.

B. Model Calibration

The presented model includes some setup-dependent parameters (k1, k_f, k_σ, k_n, k_μ, k_p, k_r) that need to be experimentally calibrated. This section presents the calibration of these parameters. It is worth to note that the model is generally applicable to different setups so long as these setup-dependent parameters are calibrated and the assumptions are satisfied.

The method used for calibration is the least-square regression using SURROGATE optimization solver in MATLAB, which is performed in the following way: 1) an objective function (Equation (21)) was defined, which aims to minimize the sum of the square of the residuals (u_{exp} is the experiment velocity and u_{pred} is the predicted velocity from the model); 2) a set of constraints for the coefficients were defined for valid value ranges of the coefficients; 3) the initial values for these coefficients were determined as the starting points of the optimization; 4) the SURROGATE function solver starts searching for a global minimum of the objective function in multiple dimensions. The calibrated values for different coefficients are listed below.

Objective function	$S = \sum_{i=1}^{n} \left(u_{exp} - u_{pred} \right)^2$	(21)

$$k_1 = \frac{54\ kg}{m^2 * s * volt} \qquad k_f = \frac{8100}{m} \qquad k_\sigma = \frac{23.6}{m} \qquad k_\mu = \frac{660\ kg}{m^2 s}$$

$$k_n = \frac{1.137e6kg}{m^2 * s^2 * volt} \qquad k_p = \frac{101}{m} \qquad k_r = \frac{1e5\ kg}{m^2 * s^2 * volt}$$

C. Model Validation

The model of predicting the nozzle exit velocity is to be validated by comparing the velocity from the model and the experiment during the entire cycle with new sets of experimental data. Furthermore, the droplet volume obtained by the integration of the theoretical velocity will be compared with the experimental volume as well. For the model of predicting the breakup time, which is defined as the instant that the filament radius becomes zero, it is to be validated by comparing with the experimental data for three different cases. Finally, the printing speed for one nozzle, which is obtained by multiplying the volume and the reciprocal of the breakup time, is also to be validated by comparing with the experimental data.

Figure 7 presents the velocity change over time for the benchmark waveform, where the same signal is repeated three times for testing the stability of the ejection in the experiments. As can be seen that the calculated experimental velocity varies largely after Tc, where the corresponding filament radius is around 1/5 of the nozzle radius. This is because the filament radius in experiments become too small as the ejection approaches to pinch-off, which causes a significant fluctuation in the velocity calculation. It is found that the ejected volume before Tc is more than 95% of the final ejected ink volume. Hence, to simplify the velocity calculation process without compromising the calculation accuracy, the velocity after Tc (R< 1/5R0) will not be presented and used in calculation for the rest of the section.

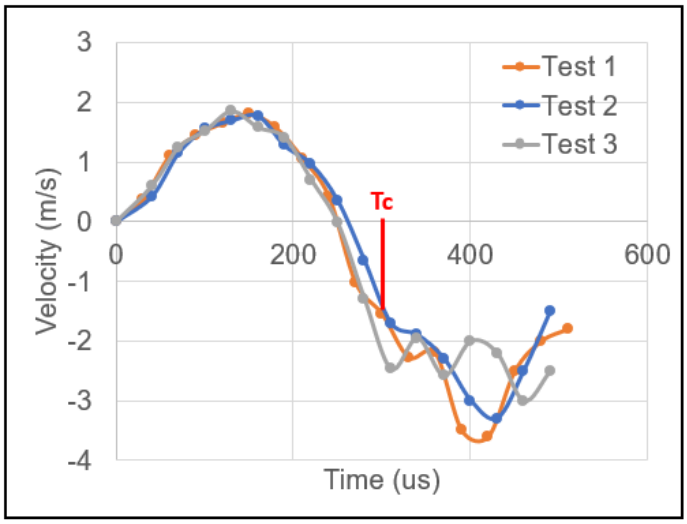

Figure 7 Velocity for the benchmark signal waveform

Figure 8 presents the velocity comparison for three different cases, where case 1 uses the benchmark signal shown in Figure 3, T2 =30us in case 2, and T3=180 us in case 3, respectively, while the rest signal parameters in case 2 and case 3 are the same with the benchmark signal. As can be seen the predicted volumes are smaller than the values in experiment in case 1 and case 2 while higher in case 3. This can be understood in the following way: as the increase of T3, the negative pressure induced by piezo in T3 decreases, which leads to a positive acceleration, as predicted in equation (13). Hence, it takes longer time for the velocity to decrease, which causes an overestimation in velocity and volume. Though discrepancies in the exact value predictions exist, these velocity trends from the model agree with those in experiment. The total ejected ink volume is obtained by the integration of velocity over time, where 7%, 12%, and 19% difference with the experimental data were observed, respectively.

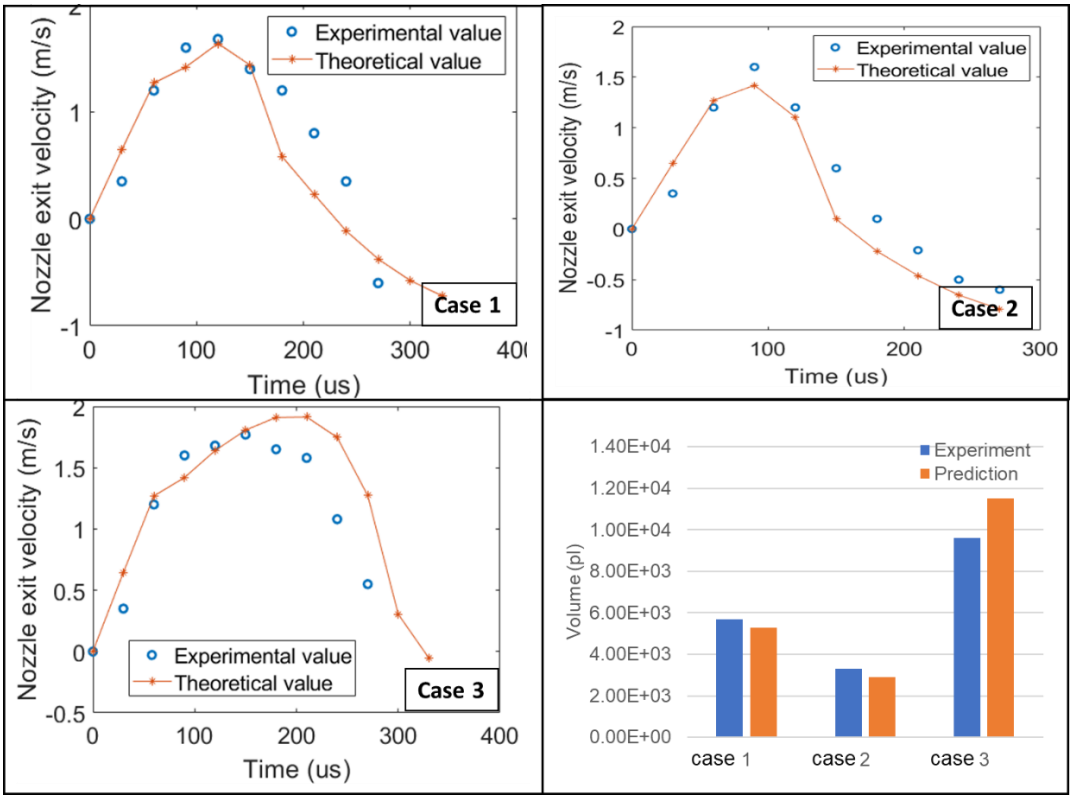

Figure 8 Velocities from theoretical prediction and experiment comparison for three different cases and their corresponding volume comparison.

Filament radius evolutions in the control volume (C.V) for the above three cases are predicted (Equation (19)) and compared with corresponding experimental measurement, as shown in Figure 9. This is used to calculate the ejection breakup time (reciprocal of the pinch-off frequency), i.e., the instant that the filament radius becomes zero. Though difference between experimental and predicted radius exists, the overall computed pinch-off frequencies for the three cases from predictions match well with experiment data, where only 2%, 3%, and 4% difference were observed, respectively.

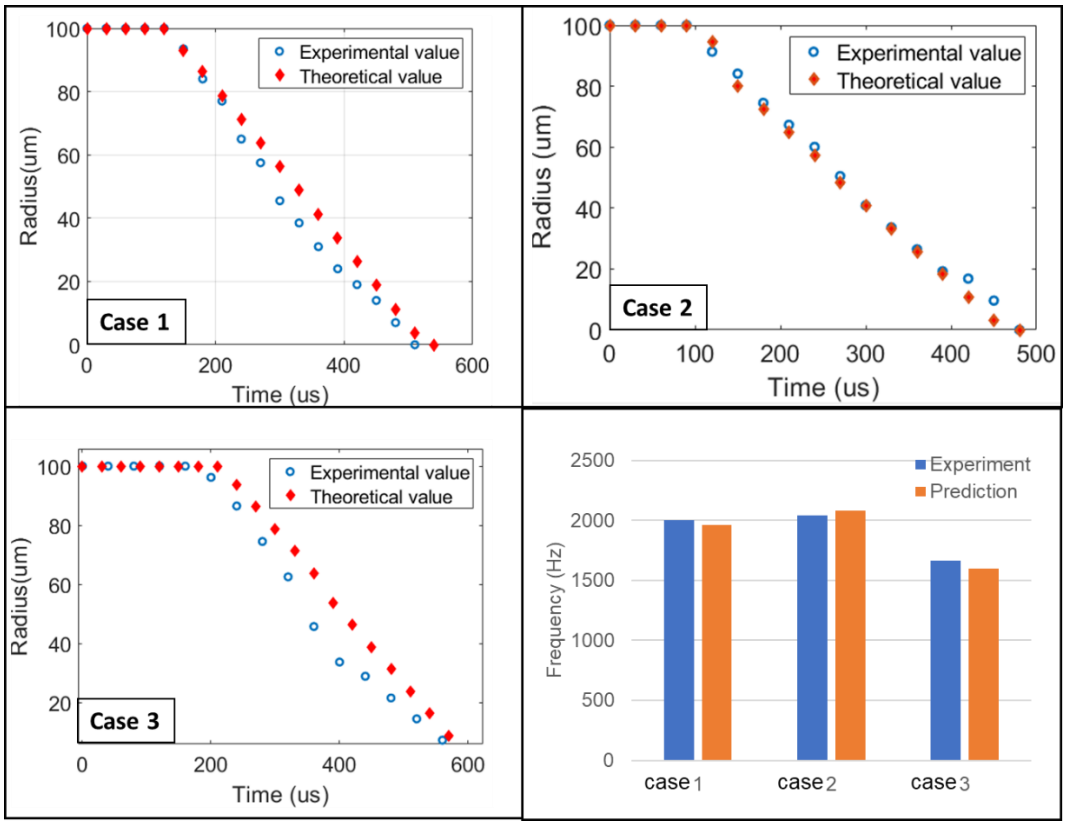

Figure 9 Radius from theoretical prediction and experiment comparison for three different cases and their corresponding pinch-off frequency comparison.

After obtaining the values of volume and frequency, based on Equation (2), the printing speed for above three cases is computed and compared with experiment data, as shown in Figure 10, where 9%, 10%, and 15% difference were observed, respectively, whereas the overall trend agrees.

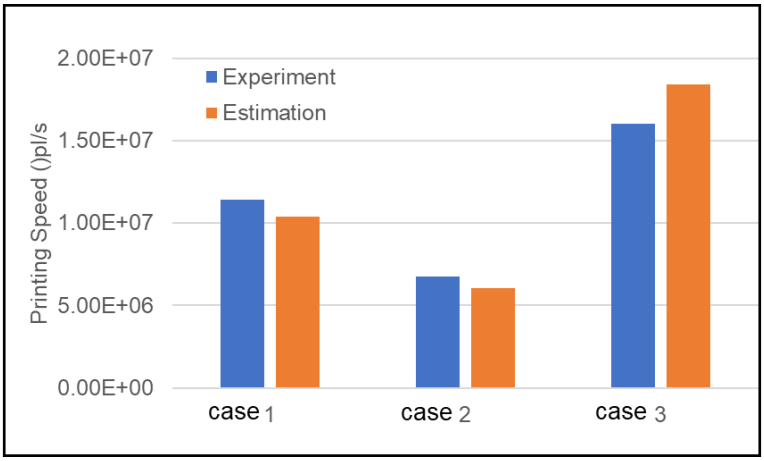

Figure 10 Printing speed comparison between prediction and experiments for three different cases

IV.SIGNAL PARAMETERS EFFECTS ON PRINTING SPEED

This section aims to investigate the effects of signal parameters on the ejected volume, breakup time, and the printings speed. To simplify this complex problem, we studied three parameters (T1, T2, and T3), which are the most important components of a typical trapezoidal signal for most of the printers. Note the signal used in this section is based on the benchmark signal (Figure 3), where only T1, T2, and T3 vary.

Figure 11 presents the predictions of the effects of T1, T2, and T3 on the breakup frequency. Generally speaking, breakup frequency decreases with the increase of T1, T2, and T3. Because the breakup time is mainly determined by the negative pressure: the earlier it starts, and/or the higher the magnitude it has, the shorter the breakup time is. With the increase of the T1 or T2, the starting time of the negative pressure is delayed, which induces a longer breakup time. With the increase of T3, the instant sucking pressure magnitude it induced becomes smaller, which would lead to a longer time for the filament to slow down and breakup. From the perspective of practical application, the signal with T2=0 might cause the pressure disturbance inside the chamber, which interferes the normal ejection eventually.

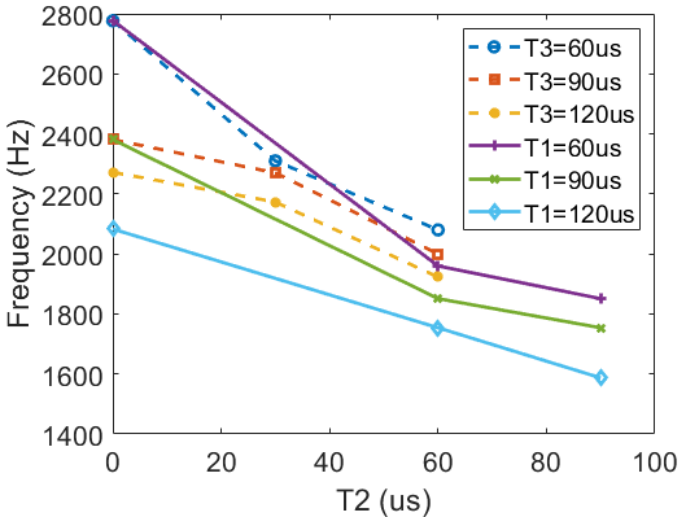

Figure 11 The estimation for breakup frequency under the effect of T_1, T_2, and T_3.

Figure 12 shows the predictions of the effects of T1, T2, and T3 on the ejected ink volume, which is obtained by performing the velocity integral in the entire process. It is found that the ejected ink volume increases with T1, T2, and T3, which is consistent with other researchers' work [38, 39]. Liu et al [38] demonstrated in simulation that for the higher T1 case, a smaller suck-back force was detected, which induced a higher volume ejection. During T2, ink keeps flowing out of nozzle due to inertia. As the increase of T2, more and more ink are ejected out of nozzle, which leads to the increase of total ejected volume. With the increasing of T3, the instant negative pressure magnitude it induced becomes smaller, which would lead to a longer time to reduce the kinetic energy of the filament, which in turn sucks less ink back and causes more ink flowing out of nozzle [39, 40]. Based on the current predictions, with the same amount of increase of these three parameters (T1, T2, and T3), the ejected ink volume increases more in T2 than in T1 and T3, which indicates that manipulating T2 is a good choice to improve the ejected ink volume.

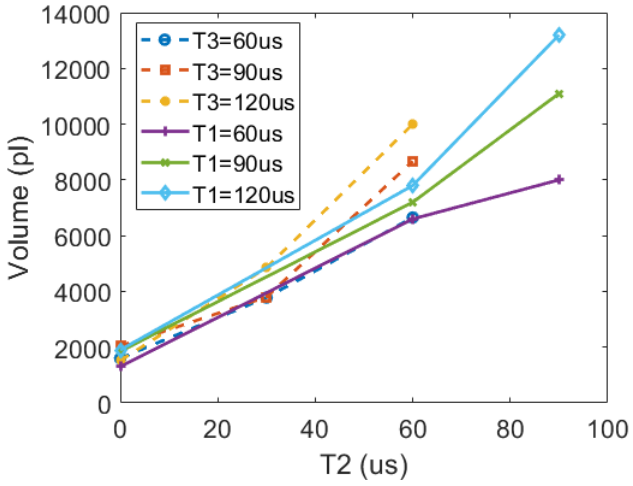

Figure 12 The estimation for ejected volume under the effect of T_1, T_2, and T_3.

By definition, printing speed for one nozzle is equal to the product of droplet volume and breakup frequency. Based on the signal effects on the breakup frequency and volume, we can estimate their effects on the printing speed (Figure 13). Even the printing speed increases with these three parameters, it seems that T2 is the most important parameter to improve the printing speed, where the highest increasing rate is observed. Note that all the predictions discussed in this section are based on reasonable ranges for T1, T2, and T3 (≤120us), where only one droplet or recombined droplet is obtained in the ejection. When these ranges were further extended, the ejected filament length would increase, which might generate one or more satellites, which is undesirable in practical applications. These undesirable situations are not covered in this paper.

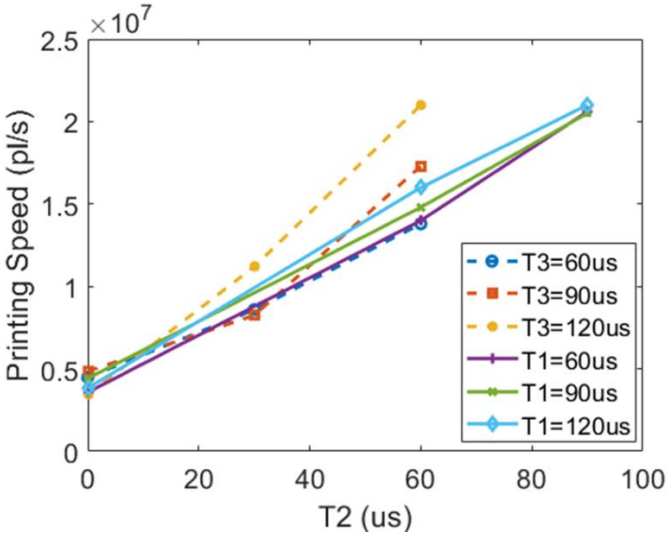

Figure 13 Predictions for printing speed under the effect of T_1, T_2, and T_3

V.CONCLUSION

This paper presented a model of the effects of the driving signal on the breakup frequency, ejected volume, and printing speed. A low-cost, high speed DOD inkjet setup is designed and developed to validate the model. Good agreements are obtained between model predictions and experimental results. Based on fundamental fluid mechanics, Navier-stokes equation is simplified and applied to the ejection process. Then equations for each stage are derived and the setup-dependent coefficients in these equations are calibrated using the least-square regression method. Validations for the model are completed through comparing the ejection frequency, volume, and printing speed with the experimental data. It is found T2 is the most important factor in the printing speed improvement. Part of our future work is to use this model to optimize the signal parameters to maximum the printing speed.

VI. Acknowledgments

We are thankful to our colleagues at the AM3 Lab for providing support and enabling environment for this work. We thank Lucas Galvan Marques for his assistance with circuit design. We gratefully acknowledge the financial support from the University of Arkansas, through the startup fund provided by the Vice Provost Office for Research and Economic Development. Any opinions, findings, and conclusions or recommendations expressed in this publication are those of the authors and do not necessarily reflect the views of the University of Arkansas.

Appendix A**: Analysis for the pressure induced by piezo moving-up**

It is assumed that piezo displacement is proportional to the voltage applied to it:

$$\Delta l = k^{*}(E_1 - E_2) \tag{A.1}$$

Thus, the average piezo speed during T3 can be estimated as

$$v = \frac{\Delta l}{t} = \mathrm{k}\frac{E_1 - E_2}{T_3} \tag{A.2}$$

Thus, at any time instant during T3 period, the piezo displacement is:

$$\mathrm{L} = vt = k\frac{E_1 - E_2}{T_3}t \tag{A.3}$$

Assuming the piezo movement to be a spherical cap, since piezo radius is much bigger than its displacement, its volume change can be written as:

$$\mathrm{volume} = \frac{1}{2}\pi L r^2 = \frac{1}{2}\pi r^2 k\frac{E_1 - E_2}{T_3}t \tag{A.4}$$

Based on Boyle's law, as volume increases, there is a proportional decrease in the pressure inside the chamber, which actually induces a stronger sucking effect for the filament, i.e., as the increase of voltage change, the induced sucking pressure increases. With the first order of approximation, this sucking pressure induced acceleration is estimated as:

$$a_n = k_n\frac{E_1 - E_2}{\rho T_3}t \tag{A.5}$$

Appendix B: **Element radius analysis at nozzle exit**

As presented in Figure 6, applying the mass conservation to the differential element at the nozzle exit, the volume in this element can be estimated as:

$$\mathrm{V} = \pi R_{i-1}^2 \Delta x + u\pi R_{i-1}^2 \Delta t - (u + \Delta u)\pi R_{i-1}^2 \Delta t = \pi R_{i-1}^2 \Delta x - \Delta u \pi R_{i-1}^2 \Delta t \quad \text{(B.1)}$$

After time Δt, volume at the control volume element with the new radius:

$$\mathrm{V} = \pi R_i^2 \Delta x \quad \text{(B.2)}$$

where R_i is the final radius of the control volume element after Δt.

Assuming the flow during this short period is steady, then the acceleration can be simplified as:

$$a_x = \frac{\partial u}{\partial t} + u\frac{\partial u}{\partial x} = u\frac{\partial u}{\partial x} = u\frac{u_{out} - u_{in}}{\Delta x} \quad \text{(B.3)}$$

Combining these three equations, the relationship between radius and velocity can be expressed as:

$$\left(\frac{R_i}{R_{i-1}}\right)^2 = 1 + \frac{a_{i-1}\Delta t}{u_{i-1}} \quad \text{(B.4)}$$

Note since the filament is inside the nozzle exit, the estimated radius cannot be bigger than nozzle radius.

Appendix C: **Custom circuit diagram**

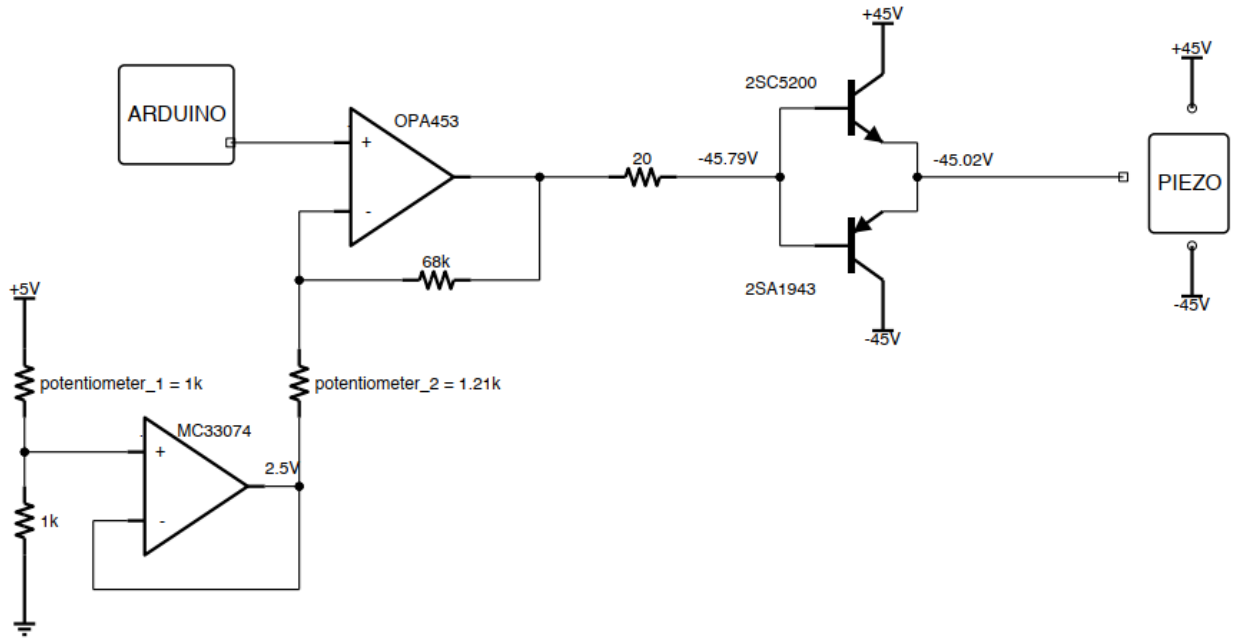

Nomenclature

f	Ejection frequency
k_1	Coefficient between acceleration and voltage change rate in T1
k_σ	Coefficient measuring the acceleration caused by capillary pressure
k_f	Coefficient measuring the acceleration caused by inertia
k_μ	Coefficient measuring the acceleration caused by viscous force
k_n	Coefficient measuring the acceleration caused by voltage change rate in T3
k_p	Coefficient measuring the acceleration caused by pressure difference between vacuum and atmosphere
k_r	Coefficient measuring the acceleration caused by piezo in T5
u(t)	Nozzle exit velocity
W	Printing speed
E_1, E_2	Voltage applied to piezo
V_1, V_2	Volume of the ejected ink
σ	Ink surface tension
ρ	Density of the ink
μ	Viscosity of the ink
R_0	Radius of the nozzle
R_i	Radius of the filament
S	Objective function

Reference

[1] I. O. f. Standardization, *Additive Manufacturing: General: Principles: Terminology*. ISO, 2015.

[2] J. K. Fink, *3D Industrial Printing with Polymers*. Newark: John Wiley & Sons, Incorporated, 2018.

[3] R. Landers, A. Pfister, U. Hubner, H. John, R. Schmelzeisen, and R. Mulhaupt, "Fabrication of soft tissue engineering scaffolds by means of rapid prototyping techniques," *Journal of materials science,* vol. 37, no. 15, pp. 3107-3116, 2002, doi: 10.1023/A:1016189724389.

[4] S. Singare *et al.*, "Rapid prototyping assisted surgery planning and custom implant design," *Rapid prototyping journal,* vol. 15, no. 1, pp. 19-23, 2009, doi: 10.1108/13552540910925027.

[5] I. Gibson, D. Rosen, and B. Stucker, *Additive manufacturing technologies: 3D printing, rapid prototyping, and direct digital manufacturing* (no. Book, Whole). Springer, 2014.

[6] G. D. Kim and Y. T. Oh, "A benchmark study on rapid prototyping processes and machines: quantitative comparisons of mechanical properties, accuracy, roughness, speed, and material cost," *Proceedings of the Institution of Mechanical Engineers, Part B: Journal of Engineering Manufacture,* vol. 222, no. 2, pp. 201-215, 2008.

[7] FUJIFILM. "Printheads Sapphire QS-256-10 AAA." (accessed 07 May, 2022).

[8] MILACRON. "MAGNA TOGGLE, A New Standard in Toggle Technology." (accessed 07 May, 2022).

[9] H. Wijshoff, "The dynamics of the piezo inkjet printhead operation," *Physics reports,* vol. 491, no. 4, pp. 77-177, 2010.

[10] MEMJET. A VersaPass Technology White Paper

[11] A. U. Chen and O. A. Basaran, "A new method for significantly reducing drop radius without reducing nozzle radius in drop-on-demand drop production," *Physics of Fluids,* vol. 14, no. 1, pp. L1-L4, 2002.

[12] A. R. Womac, J. R. Williford, B. J. Weber, K. T. Pearce, and D. L. Reichard, "Influence of Pulse Signal Spike and Liquid Characteristics on Performance of Uniform-Droplet Generator," *Transactions of the ASAE,* vol. 35, no. 1, pp. 71-79, 1992.

[13] B. V. Antohe and D. B. Wallace, "Acoustic phenomena in a demand mode piezoelectric ink jet printer," *Journal of Imaging Science and Technology,* vol. 46, no. 5, pp. 409-414, 2002.

[14] D. B. Wallace, "Drive Waveform Effects on Ink-Jet Device Performance, MicroFab Technote," in *IS&T NIP25: International Conference on digital printing technology*, 1999, no. Conference Proceedings.

[15] R. F. Burr, E. C. Segerstrom, C. M. Greb, J. M. Wiltse, and J. D. Hart, "Apparatus and method for drop size modulated ink jet printing," ed: Google Patents, 2001, p. 11.

[16] P.-H. Chen, H.-Y. Peng, H.-Y. Liu, S. L. Chang, T. I. Wu, and C.-H. Cheng, "Pressure response and droplet ejection of a piezoelectric inkjet printhead," *International Journal of Mechanical Sciences,* vol. 41, no. 2, pp. 235-248, 1999.

[17] X. Wang, "Drop-on-demand inkjet deposition of complex fluid on textiles," Georgia Institute of Technology, Dissertation/Thesis, 2008.
[18] H. Y. Gan, X. Shan, T. Eriksson, B. K. Lok, and Y. C. Lam, "Reduction of droplet volume by controlling actuating waveforms in inkjet printing for micro-pattern formation," *Journal of Micromechanics and Microengineering,* vol. 19, no. 5, p. 055010, 2009.
[19] T.-M. Liou, C.-Y. Chan, and K.-C. Shih, "Effects of actuating waveform, ink property, and nozzle size on piezoelectrically driven inkjet droplets," *Microfluidics and Nanofluidics,* vol. 8, no. 5, pp. 575-586, 2010.
[20] N. Reis, C. Ainsley, and B. Derby, "Ink-jet delivery of particle suspensions by piezoelectric droplet ejectors," *Journal of Applied Physics,* vol. 97, no. 9, p. 094903, 2005.
[21] H.-C. Wu, T.-R. Shan, W.-S. Hwang, and H.-J. Lin, "Study of micro-droplet behavior for a piezoelectric inkjet printing device using a single pulse voltage pattern," *Materials transactions,* vol. 45, no. 5, pp. 1794-1801, 2004.
[22] D. B. Wallace, "Drive Waveform Effects on Ink-Jet Device Performance, MicroFab Technote,(1999) 3 MANNING HJ, Harvey RA, Xaar greyscale technology," in *IS&T NIP25: International Conference on digital printing technology*, 1999, no. Conference Proceedings.
[23] P. Shin and J. Sung, "The effect of driving waveforms on droplet formation in a piezoelectric inkjet nozzle," in *Electronics Packaging Technology Conference, 2009. EPTC'09. 11th*, 2009, no. Conference Proceedings: IEEE, pp. 158-162.
[24] R. Self and D. Wallace, "Method of drop size modulation with extended transition time waveform," USA Patent Appl. 08/940,731, 2000.
[25] Y. Kim, W. Sim, C. Park, Y. Yoo, J. Joung, and Y. Oh, "The effects of driving waveform of piezoelectric industrial inkjet head for fine patterns," in *Nano/Micro Engineered and Molecular Systems, 2006. NEMS'06. 1st IEEE International Conference on*, Zhuhai, China, 2006, no. Conference Proceedings: IEEE, pp. 826-831.
[26] J. C. Miers and W. Zhou, "Droplet formation at megahertz frequency," *AIChE Journal,* vol. 63, no. 6, pp. 2367-2377, 2017.
[27] A. Bransky, N. Korin, M. Khoury, and S. Levenberg, "A microfluidic droplet generator based on a piezoelectric actuator," *Lab on a Chip,* vol. 9, no. 4, pp. 516-520, 2009.
[28] J. M. Meacham, M. J. Varady, F. L. Degertekin, and A. G. Fedorov, "Droplet formation and ejection from a micromachined ultrasonic droplet generator: Visualization and scaling," *Physics of Fluids,* vol. 17, no. 10, p. 100605, 2005.
[29] A. A. Goghari and S. Chandra, "Producing droplets smaller than the nozzle diameter by using a pneumatic drop-on-demand droplet generator," *Experiments in Fluids,* vol. 44, no. 1, pp. 105-114, 2008.
[30] H. Dong, W. W. Carr, and J. F. Morris, "Visualization of drop-on-demand inkjet: Drop formation and deposition," *Review of Scientific Instruments,* vol. 77, no. 8, p. 085101, 2006.
[31] G. Perçin and B. T. Khuri-Yakub, "Piezoelectric droplet ejector for ink-jet printing of fluids and solid particles," *Review of Scientific Instruments,* vol. 74, no. 2, pp. 1120-1127, 2003.

[32] J. C. Yang, W. Chien, M. King, and W. L. Grosshandler, "A simple piezoelectric droplet generator," *Experiments in Fluids,* vol. 23, no. 5, pp. 445-447, 1997.
[33] J. R. Castrejón-Pita, N. F. Morrison, O. G. Harlen, G. D. Martin, and I. M. Hutchings, "Experiments and Lagrangian simulations on the formation of droplets in drop-on-demand mode," *Physical Review E,* vol. 83, no. 3, p. 036306, 2011.
[34] K. A. Mann, S. Deutsch, J. M. Tarbell, D. B. Geselowitz, G. Rosenberg, and W. S. Pierce, "An experimental study of Newtonian and non-Newtonian flow dynamics in a ventricular assist device," 1987.
[35] H. Dong, W. W. Carr, and J. F. Morris, "An experimental study of drop-on-demand drop formation," *Physics of Fluids,* vol. 18, no. 7, p. 072102, 2006.
[36] J. Tai, H. Y. Gan, Y. N. Liang, and B. K. Lok, "Control of droplet formation in inkjet printing using Ohnesorge number category: materials and processes," in *Electronics Packaging Technology Conference, 2008. EPTC 2008. 10th*, 2008, no. Conference Proceedings: IEEE, pp. 761-766.
[37] Y. A. Çengel and J. M. Cimbala, *Fluid mechanics: fundamentals and applications*, Third ed. (no. Book, Whole). New York: McGraw Hill (in English), 2014.
[38] Y.-F. Liu, Y.-F. Pai, M.-H. Tsai, and W.-S. Hwang, "Investigation of driving waveform and resonance pressure in piezoelectric inkjet printing," *Applied Physics A,* vol. 109, no. 2, pp. 323-329, 2012.
[39] H. Dong, "Drop-on-demand inkjet drop formation and deposition," Georgia Institute of Technology, Dissertation/Thesis, 2006.
[40] H. Wijshoff, "Structure-and fluid-dynamics in piezo inkjet printheads," 2008.